Two-step immobilization of metronidazole prodrug on TEMPO cellulose nanofibrils through thiol-yne click chemistry for in situ controlled release

Hippolyte Durand, Isabelle Baussanne, Martine Demeunynck, Jasmine Viger-Gravel, Lyndon Emsley, Michel Bardet, Elisa Zeno, Naceur Belgacem, Julien Bras

Two-step immobilization of metronidazole prodrug on TEMPO cellulose nanofibrils through thiol-yne click chemistry for in situ controlled release

Hippolyte Durand[1], Isabelle Baussanne[2], Martine Demeunynck[2], Jasmine Vigier-Gravel[3], Lyndon Emsley[4], Michel Bardet[4-5], Elisa Zeno[6], Naceur Belgacem[1], Julien Bras[1]

[1] *Univ. Grenoble Alpes, CNRS, Grenoble INP, LGP2, Grenoble, France*

[2] *Univ. Grenoble Alpes, CNRS, DPM, Grenoble, France*

[3] *Department of Organic Chemistry, University of Geneva 30 Quai Ernest-Ansermet, 1211 Geneva 4, Switzerland*

[4] *Institut des Sciences et Ingénierie Chimiques, Ecole Polytechnique Fédérale de Lausanne (EPFL), CH-1015 Lausanne, Switzerland*

[5] *Univ Grenoble Alpes, CEA, INAC, MEM, Laboratoire de Résonance Magnétique, Grenoble, 38000, France*

[6] *Centre Technique du Papier (CTP), Domaine Universitaire, 38044, Grenoble Cedex 9, France*

Abstract

Nowadays, drug encapsulation and drug release from cellulose nanofibrils systems are intense research topics, and commercial grades of cellulose nanomaterials are currently available. In this work we present an ester-containing prodrug of metronidazole that is covalently bound to cellulose nanofibrils in aqueous suspension through a two-step immobilization procedure involving green chemistry principles. The presence of the drug is confirmed by several characterization tools and methods such as Raman spectroscopy, elemental analysis, Dynamic Nuclear Polarization enhanced NMR. This technique allows enhancing the sensitivity of NMR by several orders of magnitude. It has been used to study cellulose nanofibrils substrates and it appears as the ultimate tool to confirm the covalent nature of the binding through thiol-yne click chemistry. Moreover, the ester function of the immobilized prodrug can be cleaved by specific enzyme activity thus allowing controlled drug release.

Keywords

Cellulose nanofibrils, drug release, click chemistry, DNP-NMR

Introduction

Among cellulosic nanomaterials, cellulose nanofibrils (CNF) are considered as one of the best bio-sourced starting platform material for the development of unique systems. The tremendous

enthusiasm in the scientific community for this material arises from the general characteristics of cellulose nanomaterials such as widespread availability, biodegradability, biocompatibility, excellent mechanical properties and tunable surface chemistry (Kargarzadeh et al., 2018). Today, such CNF can be used in several and various applications (i.e. paper and packaging (Aulin et al., 2010; Bardet & Bras, 2014; Boufi et al., 2016; Lavoine et al., 2015), electronics (Hoeng et al., 2016), composites (Dufresne et al., 2013) medical and cosmetics (Halib et al., 2017; Jorfi & Foster, 2015; Laurén, 2018; Lin & Dufresne, 2014) industries) as reinforcement agent, rheology modifier or nanostructured networks and membranes. Among identified CNF grades, TEMPO oxidized CNF (CNF-t) has enhanced features such as its chemical reactivity together with its specific rheological properties, both explained by the presence of carboxylic acid and aldehydes moieties along the cellulose nanofibers.

Industrial production of CNF-t is under development in different places of the globe. Pioneer research investigations on TEMPO oxidation of cellulose by the group of Professor Akira Isogai in Japan (Isogai et al., 2011; Saito et al., 2006) led to the apparition of CNF-t production facilities while in Europe and North America, small companies are starting to sell CNF-t. The growing production facilities come along with novel and promising applications of CNF-t such as the biomedical field. A couple of reviews deal with the use of CNF-t (together with other cellulose nanomaterials) for biomedical application and describe the potential of this material for the design of new innovative healthcare systems (Du et al., 2019; Jorfi & Foster, 2015; Lin & Dufresne, 2014; Syverud, 2016). CNF-t draws specific attention since it is possible to produce it in an ultrapure form with low endotoxin content making them suitable for wound healing when freeze-dried into aerogels: low cytotoxicity was also confirmed in addition with really high water holding capacity (Nordli et al., 2016). CNF-t were also investigated to be used as drug carriers. The ability to deliver Ibuprofen through the skin from CNF-t-Ibuprofen gel formulations was assessed *in-vitro* and *in-vivo*. CNF-t systems were able to match with commercial references while including five times lower drug loading proving a more efficient and optimized use of drug (Celebi et al., 2016). Aerogels of different kinds of cellulose nanofibrils suspensions mixed with beclomethasone dipropionate (BDP) nanoparticle coated with hydrophobin proteins were also produced through freeze drying. CNF-t based systems showed a sustained drug release. The CNF three-dimensional structure was tunable by varying the freeze drying parameters allowing for a controlled release of the drug (Valo et al., 2013).

The antibacterial metronidazole is used to fight diseases concerning different organs and especially in gastrointestinal tract and reproductive system, mainly against anaerobic micro-organisms. Its mechanism of action involves the penetration into the anaerobic bacteria, its chemical transformation (reduction) by proteins to an active product that will cleave DNA strands, and thereby inhibits the replication mechanism thus preventing cell growth (*Metronidazole*, n.d.; Pubchem, n.d.). Since the

1980's, metronidazole has been successfully used with cellulose derivatives tableting compounds such as hydroxypropyl methyl cellulose (Campos-Aldrete & Villafuerte-Robles, 1997), methyl cellulose (Itiola & Pilpel, 1986) and cellulose acetate phthalate (Gates et al., 1994). Up to our knowledge, only a very few publications deal with the use of CNF-t and metronidazole. CNF-t hydrogels were used as matrix for encapsulation of 6 different active principle ingredients, including metronidazole. Researchers investigated the effect of freeze drying and subsequent rehydration on rheological properties and the drug release profiles. Results suggested that the CNF-t hydrogels were successfully rehydrated and release profiles were equivalent, before and after freeze drying, confirming their potential for controlled release applications (Paukkonen et al., 2017). These uses of metronidazole relied only on physical adsorption of the drug onto the cellulosic substrates. Micro and nano-sized three dimensions structures of the developed systems allowed for a diffusion-controlled release mechanism.

The purpose of this work is to prepare an enhanced CNF based drug vehicle that can be integrated in innovative implantable medical devices with controlled drug release properties. This requires a complementary anchoring strategy of the drug to the cellulosic substrates in order to achieve in situ controlled drug release. For this purpose, metronidazole was chosen as drug model as it offers two advantages. First, its chemical versatility with the pending hydroxyl group makes easy to design a new prodrug that will contain a cleavable ester linker necessary to obtain the in situ release, and a reactive thiol end-group for anchoring to the CNF. Secondly, as mentioned already, metronidazole is of first choice for anaerobic conditions, those that are met in the targeted implantation site. The presence of ester link will allow the liberation of the drug by ester-specific enzymes (present in fat tissues and on infection sites (Schakenraad et al., 1990)) on the targeted site of treatment.

On the CNF side, efficient chemical modification is required to bind the end-group of the prodrug. It should be noted that surface modification of CNF is still an intense and challenging field of research. The very large specific area of CNF, together with their high amounts of reactive hydroxyls (along with carboxylic acids and aldehydes groups in the case of CNF-t) lead to a wide range of strategies for surface modifications. Reactions such as etherification, esterification, silylation and amidation have been performed to covalently bind small molecules or polymer chains to CNF as described in relevant reviews (Habibi, 2014; Missoum et al., 2013; Rol et al., 2018). Characterization of resulting modified CNF substrates is often challenging and calls for cross characterizations, covering both chemical and physical approaches, and also functionality evaluation. The use of sustainable materials such as CNF goes hand in hand with the increasing need for low-environmental impact processes and green chemistry procedures for CNF surface functionalization. In this context, click chemistry is of particular interest. Sharpless et al. introduced in 2001 the concept of click chemistry that gathers reactions that are efficient, stereospecific, modular, requiring simple conditions (not sensible to oxygen and water),

and results quickly in very high yields while involved reagents must be readily available (Kolb et al., 2001). Click chemistry was seldom used to modify cellulose nanofibrils. CuAAC and thiol-ene click chemistry were applied to CNF films in order to immobilize fluorescent compounds (Navarro et al., 2015; Pahimanolis et al., 2011). So far, only two publications mention the use of thiol-yne click chemistry with CNF. These researcher's aim was to tailor the wettability of CNF films surface to develop fluidic channels for biosensing (Guo et al., 2018; Solin et al., 2019). In the present work, CNF was modified with a two-step chemical strategy: in the first part an alkyne group was introduced through amidation, while in the second step, the thiol-yne chemistry was used to bind the prodrug to the intermediate alkyne-CNF, as described in Figure 1.

To the best of our knowledge, this work constitutes the first example of such a sophisticated strategy towards active CNF based materials in situ release. Furthermore, the use of dynamic nuclear polarization NMR (DNP-NMR), a recent hyperpolarization technique that allows enhancing the NMR signal sensitivity by several orders of magnitude, was the ultimate tool, for the second time for our team(Kumar et al., 2020), to confirm the success of the chemical functionalization applied to cellulose nanofibrils. Its unique sensitivity allows the identification and quantification of any trace of compound, thus overcoming the challenging modified CNF characterization.

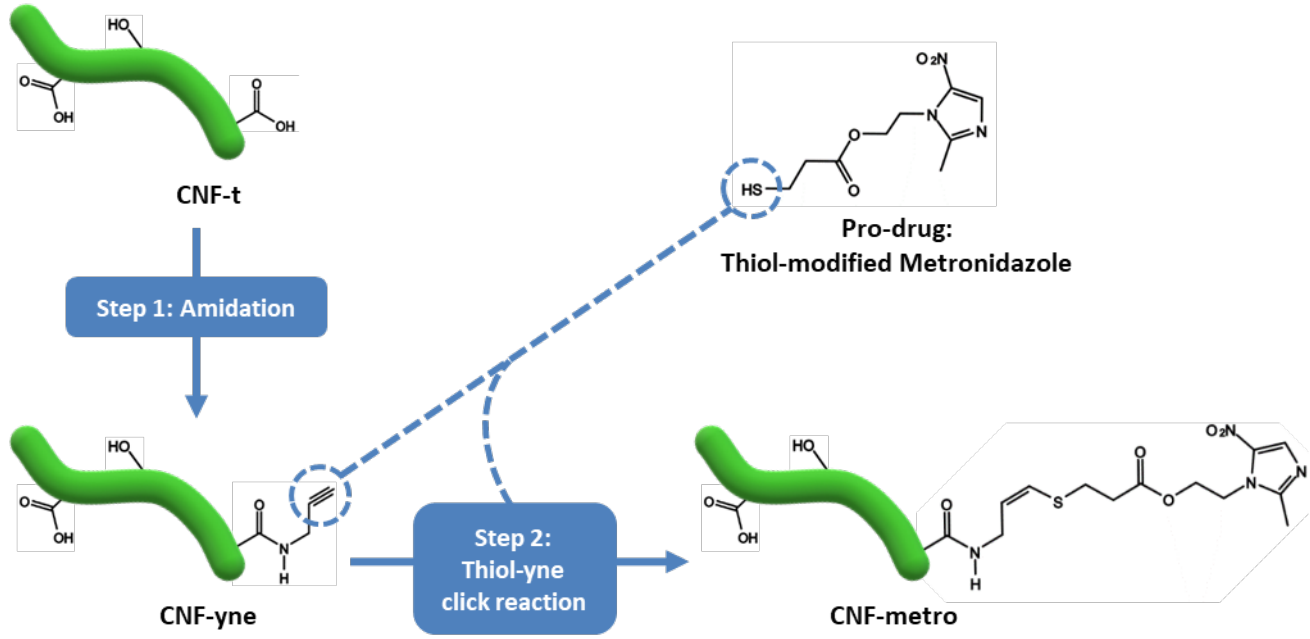

Figure 1: General multistep immobilization procedure of thiol modified metronidazole prodrug on CNF-t. Note that thiol-yne click reaction can give a double addition of thiol compound. However, due to steric hindrance, the second addition is less likely to happen so that only the "one-addition" product is depicted.

Experimental procedure

Materials

The cellulose nanofibrils (CNF) suspensions were provided by the Centre Technique du Papier (CTP, Grenoble, France). A first suspension referred as CNF-e was produced by a 2h enzymatic pre-treatment of a pre-refined (40°SR) bleached birch pulp followed by homogenization: 3 passes at 1500 bars in an Ariete homogenizer from GEA. The second suspension, which is referred as CNF-t, was also produced by the Centre Technique du Papier (CTP, Grenoble, France). The TEMPO mediated oxidation was performed on a pre-refined (40°SR) bleached bisulfite pulp provided by TEMBEC following classical procedure developed by A. Isogai's team in the end of 2000s (Isogai et al., 2011; Saito et al., 2006). The cellulose fiber pulp concentration was set at 1.5 wt% and the pre-treatment was done at pH 10 for 2h and involved NaBr, NaClO and the TEMPO reagent. The oxidized pulp was then subjected to the high pressure homogenizer (GEA Niro Soavi) to produce the CNF-t suspension.

Propargyl-amine (CAS: 2450-71-7), propargyl-bromide (CAS: 106-96-7), N-(3-dimethylaminopropyl)-N'-ethylcarbodiimide hydrochloride (EDC, CAS: 25952-53-8), N-hydroxysuccinimide (NHS, CAS: 6066-82-6), sodium hydroxide (NaOH, CAS: 1310-73-2), and hydrogen chloride (HCl, CAS: 7647-01-0) 4-(dimethylamino)pyridine (DMAP, CAS: 1122-58-3), N,N-Dicyclohexylcarbodiimide (DCC, CAS: 538-75-0), trifluoroacetic acid (TFA, CAS: 76-05-1), triisopropylsilane (TiPS, CAS: 6485-79-6) were purchased from Sigma Aldrich and used as received. Isopropanol (CAS: 67-63-0) was purchased from ACROS Organics. Tris(2-carboxyethyl)phosphine hydrochloride (TCEP, >98%, CAS: 51805-45-9) was purchased from ThermoFisher Scientific. Biocompatible photoinitiator lithium phenyl(2,4,6-trimethylbenzoyl)phosphinate (LAP, >98%, CAS: 85073-19-4) was purchased from Tokyo Chemical Industry. The biradicals 15-{[(7-oxyl-3,11-dioxa-7-azadispiro[5.1.5.3]hexadec-15-yl)carbamoyl][2-(2,5,8,11-tetraoxatridecan-13-ylamino)}-[3,11-dioxa-7-azadispiro[5.1.5.3]hexadec-7-yl])oxidanyl (AMUpol) was obtained from ICR (Aix-Marseille University, UMR7273, France). Deionized water was used for every experiment. Carboxylesterase 2 human (expressed in baculovirus infected BTI insect cells) was purchased from Sigma Aldrich and used as received. Tris(hydroxymethyl) aminomethane (TRIS, >99.8% CAS: 77-86-1) was purchased from Euromedex.

Alkynation of CNF-t through amidation

The CNF-t suspension concentration was decreased from 1.5wt% to 0.4wt% in order to be easily stirrable. Deionized water was added before homogenization with an IKA Ultra-Turrax high shear mixer (China) for 1 minute at 10 000 rpm. The pH of the suspension was then adjusted to 4 under magnetic stirring using a 0.5 M HCl solution.

A solution of the coupling agents EDC and NHS was prepared in deionized water. After complete dissolution the solution was added to the suspension of CNF-t. A molar ratio of 4 equivalents of EDC and NHS for 1 equivalent of carboxyl group of CNF-t was used. The mixture was magnetically stirred for 30 min at room temperature in order to activate the carboxyl groups of the CNF-t. The pH was maintained at 4 during the reaction with 0.5M HCl or NaOH solution droplets addition. This pH favors the EDC carbocation availability and acid form of the carboxyl groups that are both required for a better reaction.

The pH was then increased to 8.5 for the second part of the reaction i.e. the amine addition. A solution of propargyl amine was prepared in deionized water and added to the mixture. Again, a molar ratio of 4 equivalents for 1 equivalent of carboxyl groups of CNF-t was used. The mixture was magnetically stirred for 72h at room temperature and the pH was kept at 8.5 with 0.5M HCl or NaOH solution droplets addition.

After 72h of reaction, the mixture was washed by centrifugation and dialysis. First, the reaction was quenched by decreasing the pH to 2-2.5 with 0.5M HCl solution. Then, centrifugation – re-dispersion cycles were applied to the suspension: centrifugations were operated during 10 minutes at 20 000 g (about 11 100 rpm) and re-dispersions were done in acidic water (pH 2-2.5) in order to remove all the non-covalently bound chemicals (EDC, NHS and free amine). In between each centrifugation cycle, re-dispersions were done using high shear mixer (Ultra-turrax, IKA) for 1 min. A total of 6 centrifugation – re-dispersion operations were performed to ultimately isolate the alkyne modified CNF-t, referred as CNF-yne. The last dispersion was done in neutral water.

The last step of purification consisted in a dialysis of the CNF-yne suspension against neutral water with 6-8 kDA MWCO membranes (Spectra/Por® 1 Standard RC Tubing, SPECTRUM) for at least 5 days under slow magnetic stirring and renewal of the medium twice a day.

Synthesis of Metro-SH compound

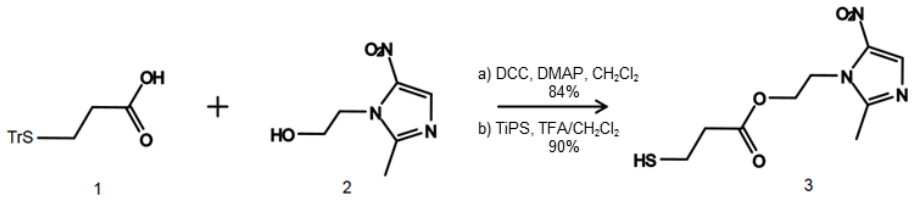

Scheme 1: Synthesis path of metronidazole-thiol (3) from Metronidazole (2) and S-trityl-3(mercaptopropionic acid (1)

The prodrug approach is a new way to investigate drug anchoring strategy to CNF. A specific prodrug need to be designed. S-Trityl-3-mercaptopropionic acid (**1**) was synthetized according to a procedure

designed by Sharma et al (Sharma et al., 2008). This product **1** (1.05 g, 3 mmol), metronidazole **2** (467 mg, 2.73 mmol) and DMAP (24 mg, 0.2 mmol) were dissolved in 30 ml of CH_2Cl_2 at 0°C. DCC (618 mg, 3 mmol) was added in the solution after 15 minutes. The reacting mixture was stirred during 3 h at room temperature, then filtered and concentrated under vacuum. The crude product was purified by flash chromatography on silica gel with CH_2Cl_2 as eluent to give the protected compound as a white solid (1.15 g, 2.3 mmol, 84 %). The tritylated compound was dissolved at 0°C in 30 ml of CH_2Cl_2 and 15 ml of TFA. After 10 minutes, TiPS (1 ml, 4.87 mmol, 2 equiv.) was added to the solution that was warmed up to room temperature and stirred for 1 h. The solution was concentrated under vacuum and the TFA was co-evaporated twice with methanol. The residue was washed three times with cold cyclohexane and dried under vacuum. The amorphous solid was purified by flash chromatography on silica gel with CH_2Cl_2/MeOH : 97/3 as eluent to give the compound **3** (**Erreur ! Source du renvoi introuvable.**) as a rosy amorphous solid. (568 mg, 95%). The full liquid ^{1}H and ^{13}C NMR characterization of the intermediate product and prodrug **3** are available in the supporting information (SI) on Figure S 1 and Figure S 2.

Immobilization of Metro-SH on CNF substrates through thio-yne click chemistry

The prodrug metro-SH **3** (62.5 mg, 0.25 mmol) was dissolved in a 15 g mixture of deionized water and ethanol (50:50 v/v ratio). To this solution, 5 ml of deionized water containing a 5% molar ratio relative to the thiol groups of **3** of tris-(2-carboxyethyl)phosphine (TCEP) (3.1mg, 0.0125 mmol), was added to prevent the air oxidation of the thiol into disulfure, and lithium phenyl(2,4,6-trimethylbenzoyl)phosphinate (LAP), a biocompatible photoinitiator required to activate the thiol-yne click reaction, was introduced at a quantity of 0.01wt% relative to the CNF-yne mass (0.02mg, $6.8E^{-5}$ mmol). Then the resulting mixture was added to the CNF-yne suspension. The whole mixture was transferred to a UV transparent two necked balloon and put under magnetic stirring. The suspension was exposed to UV radiation with a UV lamp (Fire Edge™ FE300, Phoseon Technology USA, wavelength 345-385nm) and a nitrogen flux was used to remove the dioxygen from the free volume of the balloon. The UV-exposition and nitrogen flux were maintained for 4 h. The modified CNF (CNF-Metro), was purified by several centrifugation – re-dispersion steps as described before: three steps of washing with water/ethanol mixture (50/50 v/v) and two steps with deionized water only. Washed suspensions were further purified by dialysis against deionized water under slow magnetic stirring for 5 days with daily renewal of dialysis medium in order to completely remove non-covalently bound compounds. Dialysis membranes were 6-8 kDA MWCO membranes (Spectra/Por® 1 Standard RC Tubing, SPECTRUM). CNF-Metro suspensions were stored in the fridge at 5°C before characterization. The

corresponding CNF films were produced by solvent casting in Teflon molds and let dry overnight in an oven at 40°C, these films were used for solid state characterization.

Characterization methods and tools

Atomic Force Microscopy

AFM images were recorded on a Dimension icon® (Bruker, USA). A 7,5.10^{-4} wt% suspension was prepared by several dilution of the gel using high shear mixer Ultra-Turrax (IKA). A drop of this suspension was deposited on freshly cleaved mica plate before drying overnight under fumehood at room temperature. The acquisition was performed in tapping mode using a silica coated cantilever (OTESPA® 300 kHz – 42 N/m, Bruker, USA). Zones of 3,3*3,3 µm² were analyzed.

FTIR

FTIR spectra of the films were obtained on a Perkin Elmer Spectrum One spectrometer (Waltham, Massachusetts, USA) in attenuated total reflectance (ATR) mode. At least 5 measurements of 16 scans with a resolution of 2cm^{-1} between 600 and 4000 cm^{-1} on each side of the CNF films were performed. Spectra were normalized at 1110 cm^{-1}, the approximate wavenumber of C-O-C bonds in cellulosic substrates. The most representative spectra were chosen for discussion.

RAMAN

Raman spectra were recorded on a Renishaw (INVIA, UK) spectrometer equipped with a 1200 lines/mm grating and a CCD detector. Excitation wavelength was 785 nm and the beam power was adjusted to avoid sample degradation. The incident beam was focused on the samples through an x50 ultra-long working distance objective which resulted in a spot size of an approximate diameter of 2 µm. The spectra were recorded between 0 and 3600 cm^{-1}.

Conductometric titration and DO/DS calculation

The carboxylic content of the CNF-t suspension was measured before and after the first step of functionalization by conductometric titration. The amount of CNF-t suspension corresponding to 50 mg of dry material was precisely diluted to 200 ml with de-ionized water. Magnetic stirring and high shear mixer Ultra-Turrax (IKA) were used to produce a homogeneous dispersion. The pH was decreased around 2.5 with 0.1 M HCl to turn every remaining carboxylate moieties of CNF surface into the acid form of the carboxylic acids, and the volume of added HCl solution was recorded. The titration was done with a 0.01 M NaOH solution, which precise concentration was measured with 3 colorimetric titrations before the titration of the CNF suspensions. The conductivity of the suspension was recorded after stabilization all along NaOH addition and added volumes of NaOH were reduced when the curve indicated changes in the slopes to improve the assessment of the transitions. The titration curves

typically display three regions, a first slope showing a decrease of the conductivity corresponding to the neutralization of remaining strong acid, a plateau were the weak acid groups are titrated (carboxylic groups of CNFs) and a last part where conductivity increases when all acids are titrated.

The carboxylic group content X_{ox} on CNF-t can be calculated with equation (1) and is expressed in micro-mole of carboxylic group per gram of dry CNF (µmol/g).

$$X_{ox} = \frac{C \times (V_{eq1} - V_{eq2})}{m} \quad (1)$$

The precise concentration of the NaOH solution is C. The CNF dry quantity is *m*. The two NaOH solution equivalent volumes V_{eq1} and V_{eq2} are extracted at the edge of the plateau on the titration curve by calculating the intersections of the first (decreasing slope) and third (increasing slope) part of the curve with the plateau.

The degree of oxidation (DO) represent the number of carboxylic groups per anhydroglucose unit (AGU) on oxidized CNF. It can be calculated with equation (2) according to Da Silva Perez et al. (da Silva Perez et al., 2003), and uses common terms C, m and equivalent volumes.

$$DO = \frac{162 \times C \times (V_{eq1} - V_{eq2})}{m - 36 \times C \times (V_{eq1} - V_{eq2})} \quad (2)$$

The value of 162 (g/mol) is the molar mass of the AGU. The value 36 (g/mol) is the difference between the molar mass of the carboxylate form of the carboxylic groups including the sodium counter ion (198 g/mol) and the molar mass of the AGU (162 g/mol). This term arises from the partial replacement of primary hydroxyl groups by carboxylate groups during the TEMPO mediated oxidation process.

All titrations were repeated at least three times.

Elemental analysis

CNF films were prepared by solvent casting from CNF suspensions. The suspensions were poured into Teflon molds and evaporated overnight in an oven at 40°C. Elemental Analysis was performed on a vario Micro Cube device from Elementar. Carbon, Hydrogen, Nitrogen, Sulfur and Oxygen mass proportion of CNF films were measured. Films pieces of 4 to 7 mg were weighted on a *micro-balance*. An average of four measurements was made for each sample.

Conventional NMR analyses

Liquid ^{1}H and ^{13}C NMR analyses of the new prodrug were performed at ICMG (FR2607) Chemistry Nanobio Platform, Grenoble. The results are detailed in SI.

Solid state ^{13}C nuclear magnetic resonance (^{13}C ssNMR) analyses were performed at the « Institute for Nanoscience and Cryogenics (INAC) » in the «French Alternative Energies and Atomic Energy Commission (CEA) » at Grenoble, on a Bruker AVANCE400 spectrometer. Acquisition, data treatment and peaks deconvolution were done using the LINUX TopSpin 3.2 software. Samples were placed in 4 mm ZrO_2 rotors. All spectra were recorded using a combination of cross-polarization (CP), high power proton decoupling and magic angle spinning (CP/MAS). ^{13}C NMR spectra were acquired at 298 K, with a 4 mm probe operating at 100.13 MHz. The chemical shift values were measured with respect to TMS via glycine as a secondary reference with the carbonyl signal set to 176.03 ppm. MAS was performed at 14 kHz. The number of scans was 15 000 with a recycle delay of 2 s and CP time of 1.5 ms.

Dynamic Nuclear Polarization – NMR (DNP-NMR)

DNP experiments were performed on a 263 GHz/400 MHz AVANCE III Bruker DNP system at the « École Polytechnique Fédérale de Lausanne (EPFL) ». The spectrometer is equipped with a low temperature MAS probe and a 263 GHz gyrotron capable of outputting ca. 5-10 W of CW microwaves. The probe was configured in double mode $^{1}H/^{13}C$. The sweep coil of the main magnetic field was optimized so that microwave irradiation gave the maximum positive proton DNP enhancement for AMUPol (a biradical polarizing agent). Proton and carbon DNP enhancements were determined by comparing the intensity of their respective spectra acquired with and without microwave irradiation. For DNP experiments, 30 mg of sample is impregnated with 16 µl of 10 mM AMUPol in D_2O/H_2O (9/1 v/v). The DNP sample is then packed in a 3.2 mm sapphire rotor and capped with a Teflon plug and zirconia cap. The filled DNP rotor was then spun at room temperature in the spinning station up to 12.5 kHz before being inserted into the pre-cooled (ca. 100 K) 3.2 mm low temperature MAS NMR probe, where the sample is frozen within a few seconds.

For ^{13}C NMR experiments, the recycle delays were 3 or 4 s. The ^{1}H $\pi/2$ pulse length used for the variable amplitude CP experiments was 2.5 µs to afford 100 kHz ^{1}H decoupling using SPINAL-64 (Fung et al., 2000). The contact time was typically 5 ms. The MAS frequency used is 12.5 kHz.

For the 1D and 2D INADEQUATE experiments the corresponding sequences are those of TOPSPIN, the NMR software proposed by Bruker Corporation. The 2D ^{13}C-^{13}C INADEQUATE is the version proposed by Lesage et al. adding DNP conditions (Cadars et al., 2007; Lesage et al., 1999). Tau delay, synchronized with the rotation, was optimized and set to 4 ms. The number of scans was set to 64 and

the number of experiments in the indirect dimension to 128 and the recycling delay to 3s leading to an experiment time in the range of 8 h.

Drug release in enzymatic medium

In order to confirm the controlled drug activation, the enzymatic release of metronidazole was assessed from the suspension of CNF-metro. It was induced by the addition of a human carboxylesterase 2 (hCE2), inspiring from a recent work with similar enzymatic release strategy (Bliman et al., 2018). This enzyme favors the cleavage of the ester bond that binds metronidazole to the CNF-metro and prodrug arm. CNF-metro suspension was centrifuged at 20 000 g for 10 min and re-dispersed in TRIS buffer (pH 7.4, 50 mM). This operation was repeated 2 times. A volume of 10 ml of CNF-metro suspension was poured into a balloon and heated at 37°C. The commercial enzyme solution was diluted to 1 mg/ml with TRIS buffer and 2 ml of this solution was introduced in the CNF-metro suspension. The mixture was maintained under magnetic stirring and at 37°C for 48 h. In parallel, a 10 ml CNF-metro suspension without the enzyme (also re-dispersed in TRIS buffer) was exposed to the same condition, acting as a reference. Aliquots were collected from both balloons in order to assess the influence of the enzyme addition on the release of the metronidazole. 500 µl aliquots were collected at predetermined time intervals and centrifuged at 14 000g for 10 min and filtrated with syringe filter (0.45 µm, polyamide/nylon, CHROMAFIL AO-45/3 MACHEREY NAGEL) before characterization. Reverse-phase high performance liquid chromatography (HPLC) was performed with a micro-bondapak-C18 analytical column (Waters Associates) to track the presence of metronidazole in the aliquot. A Waters chromatographic system was used, with two M-510 pumps and photodiode array detector Waters 996 using Millenium 32 software. A linear gradient from 10 to 100 % methanol in H_2O pH 2.5 (phosphoric acid), 1 ml/min flow rate, was used.

Results and discussions

Characterization of CNF-t starting materials

Considering the numerous commercially available CNF types and the wide variety of lab-scale produced CNF, it is of high importance to precisely describe the properties and characteristics of the CNF that are used in this work. Cellulose nanofibrils suspensions are often a mixture of nanoscale particles, microfibrillated fibers, aggregates and residual fibers. The objective is to understand the starting material and be able to draw relevant conclusions from the presented results.

The CNF-t suspension that was produced by the CTP has the appearance of a thick transparent gel at 1.6wt% concentration as depicted on Figure 2 . AFM images of the low concentrated CNF-t suspension

were also recorded in order to confirm the nanosize morphology of cellulose nanofibrils, as depicted on **Erreur ! Source du renvoi introuvable.**b.

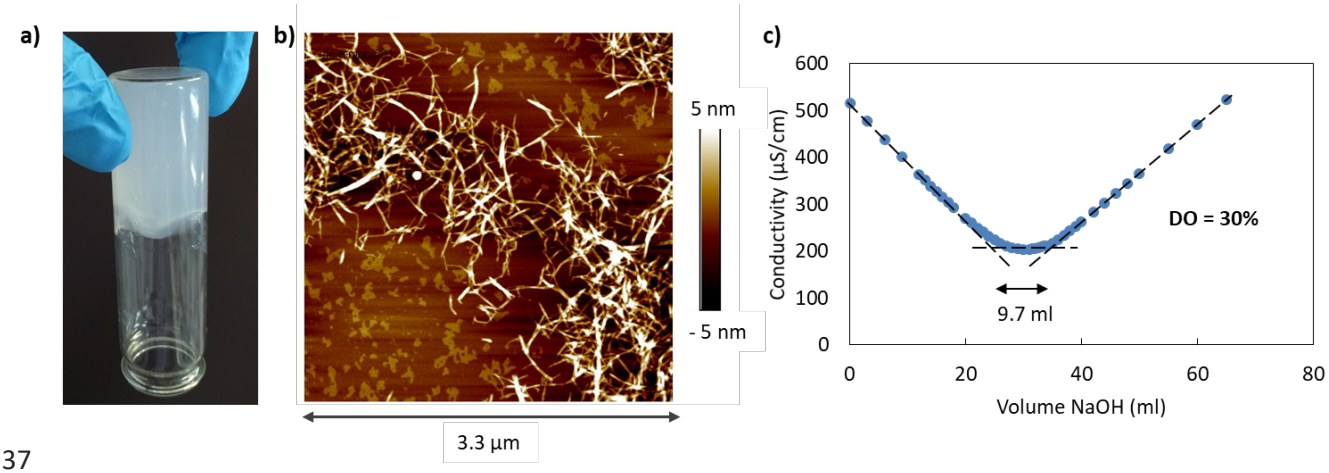

Figure 2: CNF-t starting material characterization: a) picture of the thick 1.6 wt% gel, b) an AFM height sensor image of a 15.10^{-5} wt% suspension and c) results of the conductometric titration (DO: degree of oxidation)

In order to assess the chemical reactivity of the CNF-t suspension, conductometric titration was performed to measure the degree of oxidation (DO) and initial carboxylic acid group content X_{ox}. A degree of oxidation of 30% and quantity of 1.7 mmol/g ± 0.1 of carboxylic acid group was detected, which confirmed the high surface charge arising from TEMPO-mediated oxidation.

First step: Introduction of alkyne function through amidation

The first reaction of the two-step immobilization procedure involves the CNF-t gel, on which an amidation reaction was performed with propargyl amine to tether pending alkyne groups. After purification steps, characterization of the grafting was made, either by analyzing the resulting CNF-yne suspension or CNF-yne dry films produced by solvent casting. Characterization techniques allowed to confirm the presence of the propargyl amine and/or the covalent nature of the bond between CNF-t and propargyl amine. We will first present the data that indicate the presence of alkyne groups, and then discuss the data confirming the covalent nature of the bond and the success of the amidation.

Spectroscopies

Chemical structure of the resulting CNF-yne dry films was investigated through FTIR spectroscopy in ATR mode. The surface of the films was then analyzed in order to reveal new chemical bonds. **Erreur ! Source du renvoi introuvable.**a shows FTIR spectra of CNF-t, CNF-yne and CNF-Metro. The three spectra showed classical peaks for cellulose backbone: stretching of O-H and C-H bonds around 3300 cm^{-1} and 2900 cm^{-1}, C-O-C glycosidic bond stretching at 1160 cm^{-1} and C-O bonds at 1100, 1050 and 1030 cm^{-1} (Johan Foster et al., 2018). CNF-t IR spectrum also showed two clear peaks at 1602 cm^{-1} and 1715 cm^{-1} that were respectively associated with C=O of carboxylate and carboxylic acid groups. The

pH of the CNF-t suspension was adjusted to 3 before producing films for analysis thus explaining the presence of carboxylic acid group signal. CNF-yne also showed the same peaks but with a lower intensity. Moreover, another peak arising around 1655 cm^{-1} was attributed to the C=O bond of amide I function, and a weak signal around 1550 cm^{-1} was due to to the C-N bond of amide I function (Hoeng et al., 2015). These data qualitatively proved the successful amidation reaction. Recent papers on amidation of CNF-t showed similar behavior in FTIR experiments and based their main conclusions on this characterization tool (Lavoine et al., 2017). In our case, as the shifts were limited, complementary characterizations were performed.

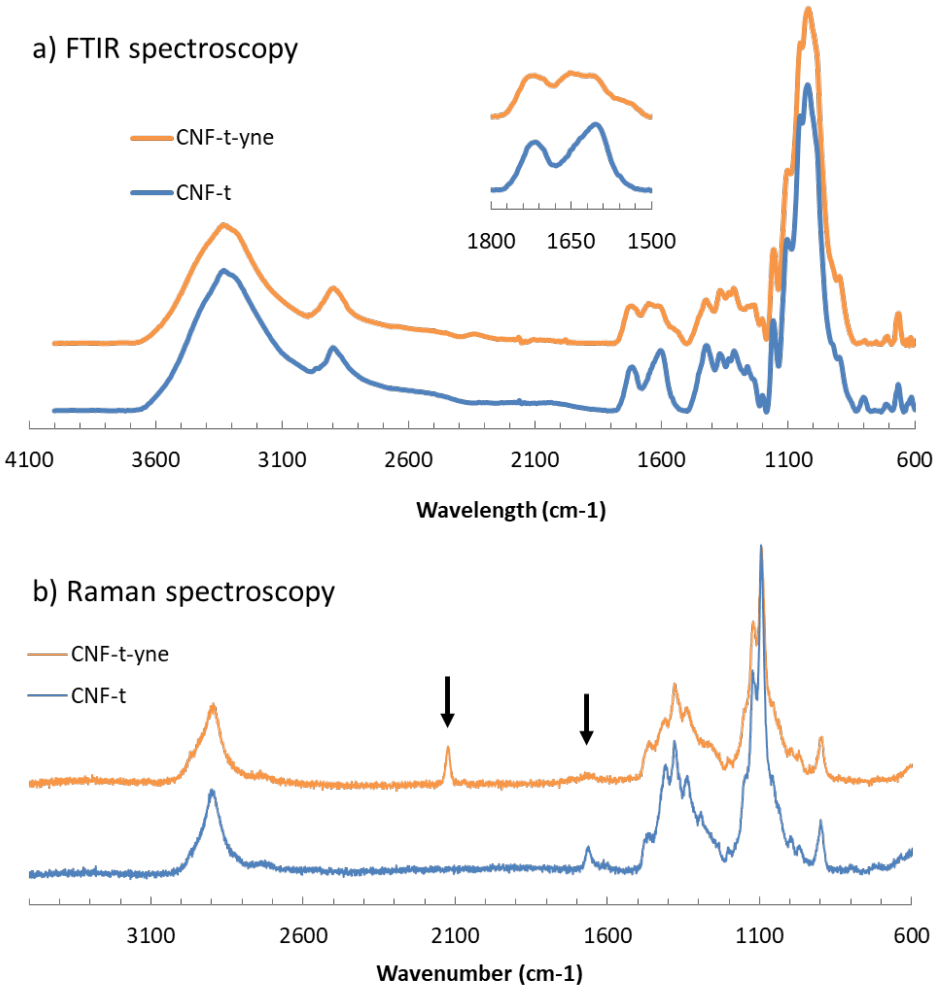

Figure 3: Spectroscopy results for a) FTIR-ATR and b) Raman spectra of CNF-t and CNF-yne samples

While FTIR spectroscopy relies on the study of absorption or transmission of light on a wide range of wavelength, Raman spectroscopy relies on the study of the inelastic scattering of a specific wavelength light beam. This technique is complementary to the FTIR spectroscopy because some chemical bonds are much more active in Raman spectroscopy and could hardly be detected with FTIR spectroscopy and vice versa, especially when the proportion of the expected bond is low. This is the case of alkyne bonds, which appeared to be more sensitive to Raman spectroscopy than in FTIR (Mangiante et al.,

2013). The Raman spectroscopy spectra are shown on **Erreur ! Source du renvoi introuvable.**b. Both spectra showed characteristic peaks of cellulosic materials: C-H stretching at 2900 cm^{-1} and C-O bridges around 1100 cm^{-1} (Agarwal, 2017). On CNF-t spectrum, the peak at 1660 cm^{-1} referred to the C=O of carboxylic acid groups. A clear signal appearing at 2120 cm^{-1} was attributed to the C≡C bond on the grafted propargyl-amine moiety (Mangiante et al., 2013). This signal was not detected on the ATR-FTIR spectra. Moreover, the signal of the C=O of the carboxylic acid was slightly flatten indicating its partial conversion to amide group. This Raman spectroscopy analysis further confirmed the success of the amidation.

Conductometric titration results

After the amidation reaction with propargyl amine, the remaining carboxylic group were also quantified by conductometric titration and the residual degree of oxidation DO_{res} was calculated with equation (3) (detailed in SI) by integrating the molecular weight of the propargylamine and the same previous terms as it was done before on cellulosic nanomaterials (Hoeng et al., 2015).

A value of 9% of residual carboxylic acid content DO_{res} was obtained. According to equation (4) (detailed in SI), a proportion of 69% of initial carboxylic acid groups converted to amide function. This first quantitative result indicates that more than two-third of the carboxylic acid moieties reacted to become amide function**.** From the values of X_{ox} and $\%COOH_{conv}$ obtained with equations (3) and (4), it was possible to calculate with equation (5) a degree of substitution based on conductometric titration measurements DS_{cond} (detailed in SI). The degree of substitution based on conductometric titration was calculated with equation (5) and revealed to be DS_{cond} = 0.19, which is in accordance with commonly reported results for this kind of heterogeneous chemical grafting (Missoum et al., 2013; Rol et al., 2018).

Solid state ^{13}C NMR

It was also used to further identify the composition of CNF-t and CNF-yne. The full signals of solid state ^{13}C NMR are available in SI and display the expected peaks for cellulose based material. The discussion here will focus on the 165-180 ppm region where carboxyl signals are usually detected. Deconvolutions of the ^{13}C NMR signals for CNF-t and CNF-yne are showed on Figure 4. The peak at 174 ppm was associated with the carbon of the carboxylic acid groups of CNF-t (Montanari et al., 2005). This peak was slightly shifted on CNF-yne signal, indicating a change of chemical environment due to the amidation reaction. A deconvolution technique was applied to unveil the contributions that explain this shift. After deconvolution, the experimental CNF-yne signal displayed on Figure 4d can be simulated by a combination of carboxylic acid and amide model contributions. The overlap obtained

was as high as 98.72%, confirming the formation of the amide function on the CNF-t and the successful covalent immobilization of alkyne function on CNF.

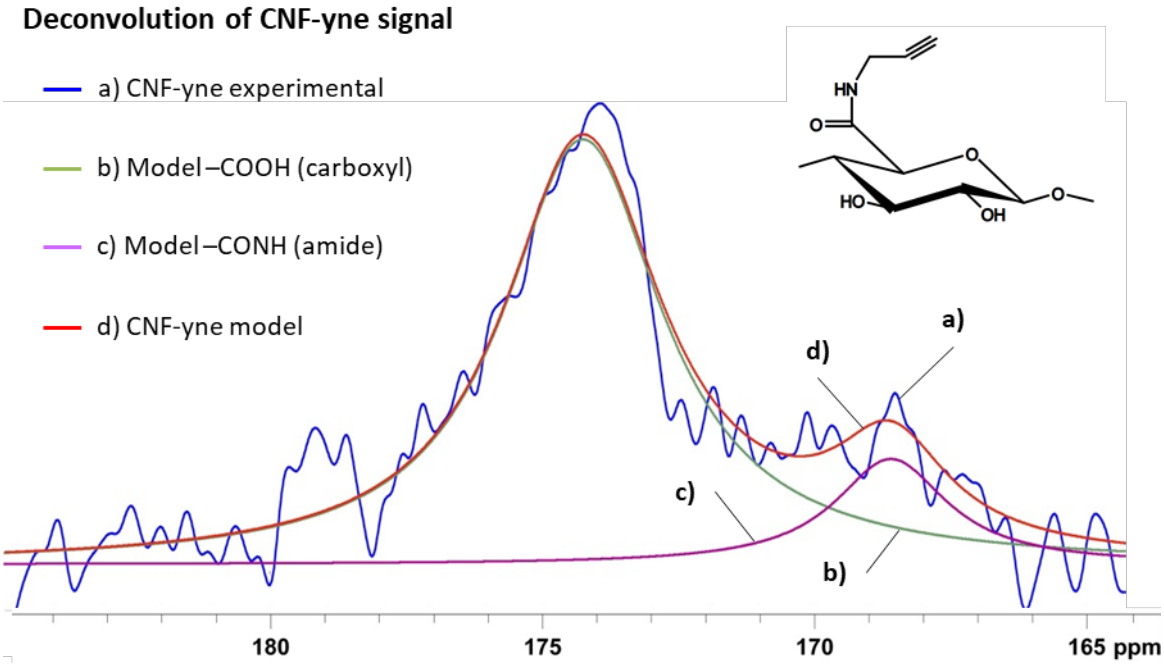

Figure 4: Deconvolution of solid state ^{13}C NMR signal for CNF-yne, a) the experimental signal, b) and c) the model carboxyl and amide signals respectively and d) the calculated signal after deconvolution based on b) and c)

Dynamic nuclear polarization enhanced NMR (DNP-NMR)

This hyperpolarization method can increase sensitivity of solid state NMR by several orders of magnitude (Rossini et al., 2013). As a proof of its potential, Figure 5 compares the spectra of CNF-t without and with the microwave (MW) irradiation that allows the dynamic nuclear polarization transfer. The acquisition time of such signals is also very fast in comparison with conventional solid state NMR. When several hours are necessary to increase signal to noise ratio in conventional solid-state NMR, only minutes-long acquisition of DNP enhanced NMR result in sharp and fine signals. As a matter of fact, in this example we could reach a 55 fold enhancement of signal to noise ratio. On a practical point of view in order to reach similar signal to noise ratio without DNP technique it would have been necessary to multiply the number of accumulated transients by 3000. This is the reason why 2D ^{13}C INADEQUATE experiments in the solid phase become possible in natural abundance.

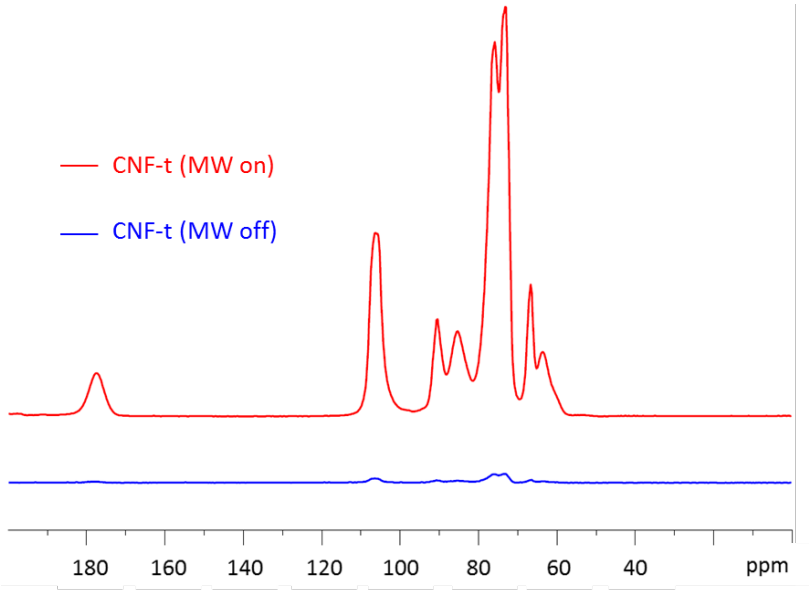

Figure 5: ^{13}C DNP-NMR spectra for CNF-t, with (red) and without(blue) microwave irradiation(µwave)

The first result arising from DNP enhanced NMR was a further confirmation of the success of the amidation. Well defined signals appeared on CNF-yne spectra of Figure 6a. Two peaks around 32 and 38 ppm were attributed to the aliphatic -CH_2- carbons introduced with propargylamine immobilization on CNF-t. These peaks were barely visible on conventional solid-state NMR. The carbons involved in the alkyne function are not visible since they are supposed to be located around 70-79 ppm, which overlaps with the C2, C3 and C5 of cellulose backbone.

Moreover, as explained above, DNP enhanced NMR allows the acquisition of 2D INADEQUATE ^{13}C-^{13}C analysis with ^{13}C natural abundance. For instance, this analysis was used to study the region of carbons involved in carbonyls of CNF-t and CNF-yne samples. Figure 6b shows the shift in the signal indicating the presence of a new type of carbon. This result confirmed the deconvolution treatment described above regarding the apparition of a signal due to the amidation reaction. This further proves the success of the amidation reaction.

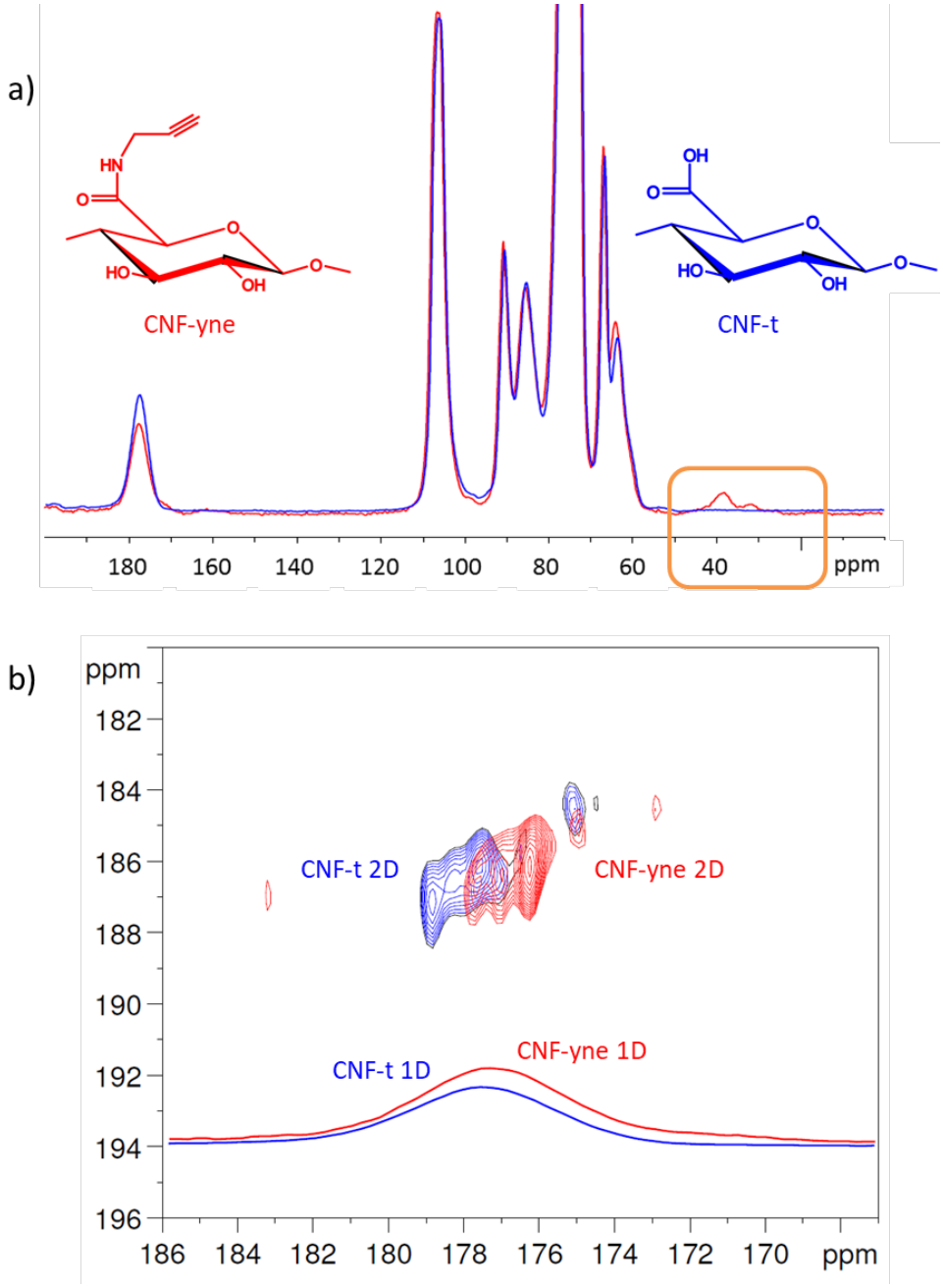

Figure 6: a) ^{13}C DNP-NMR spectra of CNF-t and CNF-yne. Aliphatic -CH_2- carbons arises from CNF-yne signal anb b) 2D ^{13}C-^{13}C inadequate DNP-NMR analysis of CNF-t and CNF-yne. The shift indicates the apparition of a carbon involved in an amide function.

Second step: thiol-yne click chemistry reaction

The second step of the grafting strategy involved a click reaction to anchor the thiol-modified Metro-SH to the CNF-yne. As depicted in Figure 1, the CNF-metro product displays only one molecule of thiol-modified drug per residue while the alkyne group is supposed to bind up to two thiol containing molecules by thiol-yne click reaction. However, considering the strong steric hindrance and the heterogeneous conditions of the chemistry that happened here, the binding of two molecules on the

alkyne group is probably strongly disfavored. We therefore depicted the result of the single addition even if double addition was not completely ruled out.

Elemental analysis

Carbon, hydrogen, nitrogen and sulfur mass proportion were measured for each sample. Elemental composition is available for the first step amidation reaction. However, the amount of nitrogen arising from the new amide function competes with the amount of nitrogen contained in potential residual adsorbed coupling agents EDC/NHS and reaction by-products such as EDC-urea and NHS-ester, despite thorough washing steps (Fujisawa et al., 2011; Kumar et al., 2020). The detection of nitrogen on CNF-yne, compared to CNF-t, supports the presence of the propargyl amine and its alkyne function at best. Nevertheless, when it comes to discuss the outcome of the thiol-yne click chemistry, elemental analysis provided more robust information, especially for sulfur atoms since they are introduced for the first time in the chemical sequence. Considering the amount of nitrogen and sulfur atoms that were theoretically introduced at this second step, the confirmation of the presence of the Metro-SH on the CNF-yne was clearly set. In fact on Table 1, a significant increase of nitrogen content in comparison with the CNF-yne was detected, going from 1.15 % ±0.05 to 1.42 % ±0.03. Moreover, in the second step, no nitrogen-containing chemical agents were introduced confirming that the increase of this element is only due to the presence of Metro-SH. In parallel, sulfur was also detected at 0.37% ±0.01 while it was not detectable on CNF-yne. Also, the final ratio between the quantity of nitrogen and sulfur atoms must be close to 4 according to the chemical structure of CNF-Metro. The elemental analysis results gave a ratio of 1.42/0.37 = 3.8, which roughly fits with the expected result. The progressive increase of nitrogen and the detection of sulfur both confirmed the immobilization of the Metro-SH onto the CNF.

Table 1: Elemental analysis results for carbon, hydrogen, nitrogen and sulfur mass proportion of the various CNF samples

	% C	*sd*	% H	*sd*	% N	*sd*	% S	*sd*
CNF-t	**37.04**	*0.02*	**5.34**	*0.18*	**< 0.10**	-	**< 0.10**	-
CNF-yne	**40.59**	*0.13*	**5.69**	*0.22*	**1.15**	*0.05*	**< 0.10**	-
CNF-metro	**40.99**	*0.04*	**6.02**	*0.09*	**1.42**	*0.03*	**0.37**	*0.01*

Solid state ^{13}C NMR

^{13}C NMR was used to further identify the composition of CNF-metro sample. On **Erreur ! Source du renvoi introuvable.**4, in the region corresponding to carbons involved in C=O around 170 ppm, we noticed a difference of the shape of the CNF-yne signal suggesting a new chemical environment. The deconvolution technique was used again to clarify this result. The CNF-metro model signal (red) displayed on Figure 7 perfectly fits with the low signal to noise experimental signal of CNF-metro (blue). A combination of model carboxylic acid, amide and ester contributions allowed the overlap to reach 98.9%, confirming indirectly the presence of an ester function. The thiol-modified drug is the only compound that contained such a chemical function. This is a complementary proof that the immobilization of the modified metronidazole on the cellulosic substrate was successful.

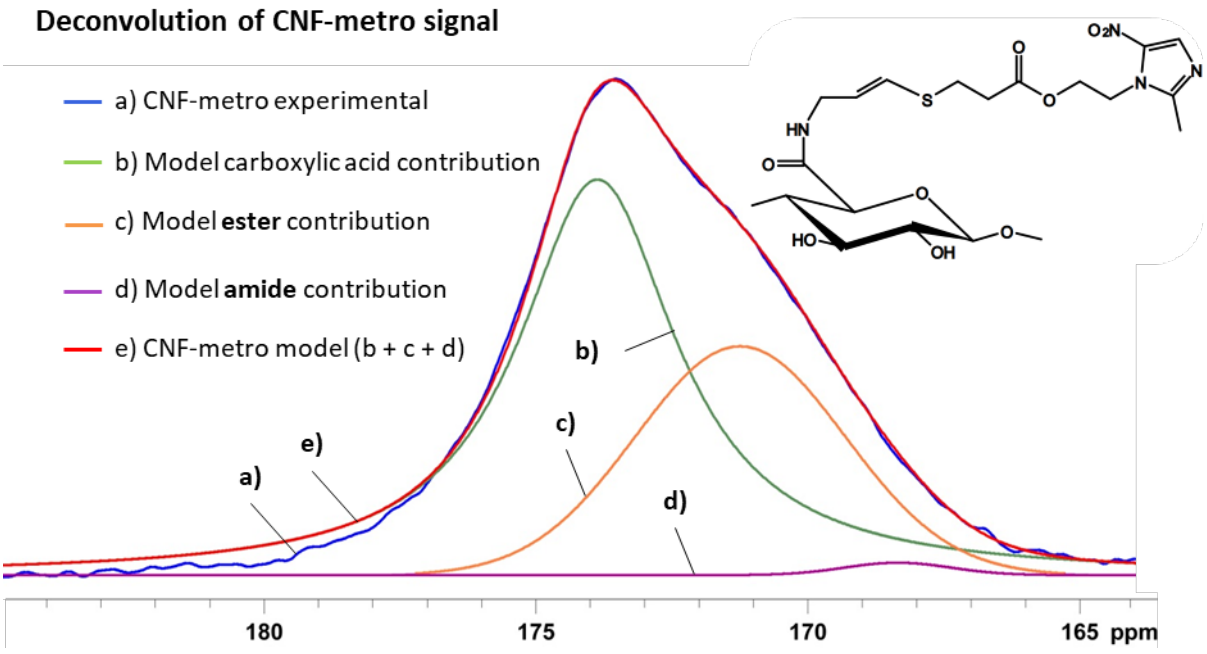

Figure 7: Deconvolution of solid state ^{13}C NMR signal for CNF-metro, a) the experimental signal, b), c) and d) the model carboxyl, ester and amide signals respectively and e) the reconstructed model signal based on b), c) and d)

Dynamic nuclear polarization enhanced NMR (DNP-NMR)

CNF-metro was also analyzed with DNP-NMR. Similarly to the previous conventional NMR signal discussed above, a shift can be noticed in the carbonyls region around 175 ppm on Figure 8a, which suggests the same modification of chemical environment for CNF-metro. The analysis provided access to the superfine signals hidden in the noise of conventional solid state NMR as clearly displayed on Figure 8b. In order to perform the attribution of each new detected peak in CNF-metro signal, the

liquid NMR spectrum of thiol-modified metronidazole was added in red. A JMOD sequence was used to facilitate the attribution of carbons involved in -CH- and -CH_3- functions since they appear with opposite phase compared to CH_2 signals. The peaks that arise around 12 ppm and 128 ppm were thus easily attributed to C7 and C8. Moreover, C9 carbon matches the peak of CNF-metro at 150 ppm. These peaks indicate again the immobilization of the prodrug molecule on the CNF-metro samples. However, the nature of the grafting was still to be confirmed since both covalently bound prodrug and adsorbed prodrug can be present.

Finally, the C1 signal at 21 ppm on Metro-SH red signal on Figure 8b was not visible on the spectrum of CNF-metro, despite the enhanced sensitivity of DNP. In parallel, we can observe a wider signal for -CH2- in comparison with CNF-yne spectrum between 25 and 45 ppm. The C1 signal has been shifted to higher chemical shifts and this is fully consistent with the thiol-yne reaction that replaced the proton on the sulfur atom by an -CH=CH- group. These results are a good indication of the covalent nature of the binding of the prodrug molecule to the alkyne groups of the CNF substrate through thiol-yne click chemistry. This study also highlighted the unprecedented potential of DNP-NMR to detect very small differences in solid material functionalization. This technique allowed us to unambiguously confirm the two-step covalent immobilization of the prodrug on cellulose nanofibrils substrate in aqueous media.

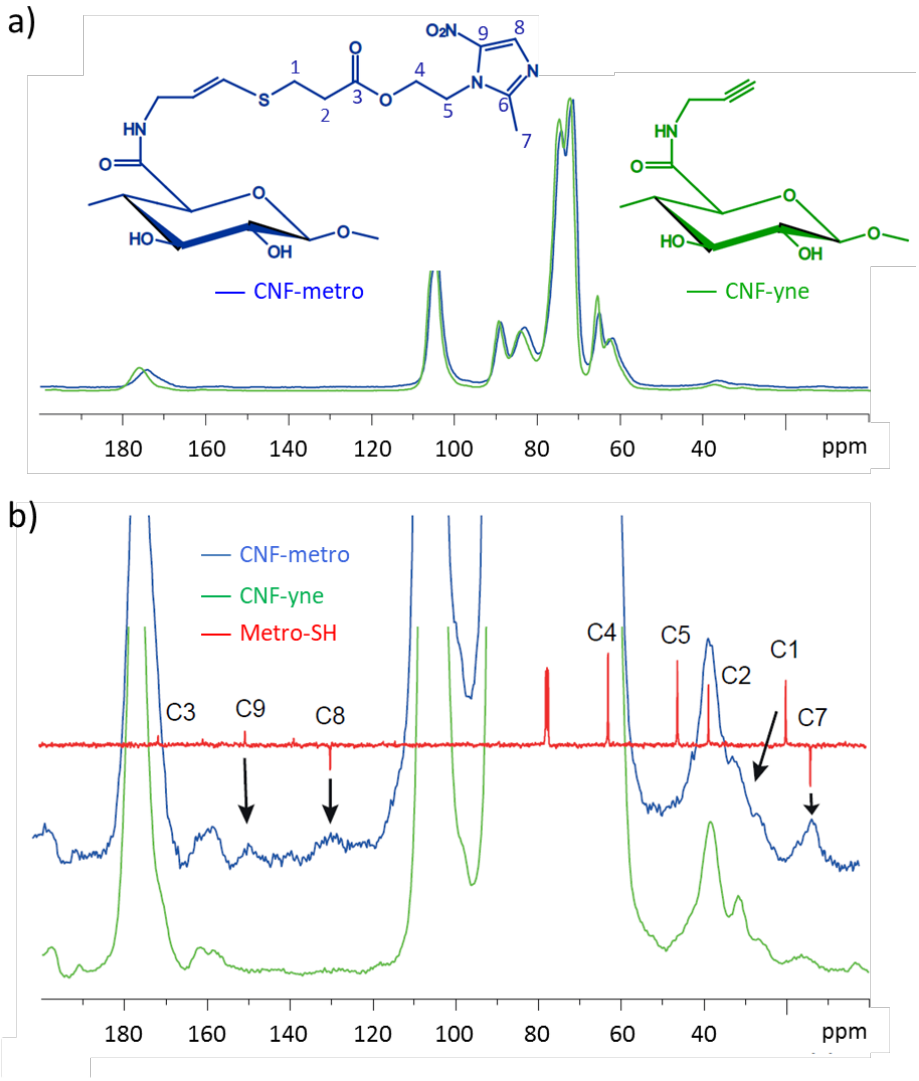

Figure 8: a) DNP enhanced ^{13}C NMR of CNF-yne and CNF-metro samples and b) the same signals completed with the liquid ^{13}C NMR spectrum of the prodrug Metro-SH containing the metronidazole molecule, a JMOD sequence was used to give negative -CH- and $-CH_3-$ signals

Proof of concept: esterase catalyzed in situ drug release

The release of metronidazole under enzymatic stimuli was analyzed. Indeed, infection sites have important enzymatic activity that may be useful for prodrug activation through ester bond cleavage. Two suspensions of CNF-metro were maintained at 37°C for 48 h under magnetic stirring. Human carboxylesterase 2 was added in one of the two suspensions for releasing the metronidazole grafted on CNF substrate, through the cleavage of the ester function. Aliquots of the suspensions were analyzed by HPLC analysis. After 1 h of agitation, a clear signal with a 3.7 minute retention time (RT) was obtained with the suspension that contains the enzyme, as illustrated on Figure 9a. By comparison with the HPLC data of metronidazole itself (results not shown), this signal (both RT and UV-Visible maximum at 283.9 nm) can be attributed to the release of the metronidazole. The CNF-metro

suspension that was gently stirred in the absence of the enzyme was also analyzed with HPLC. However, even after 4 h, no trace of the metronidazole was detected as confirmed by both the chromatogram and UV spectrum of Figure 9b.

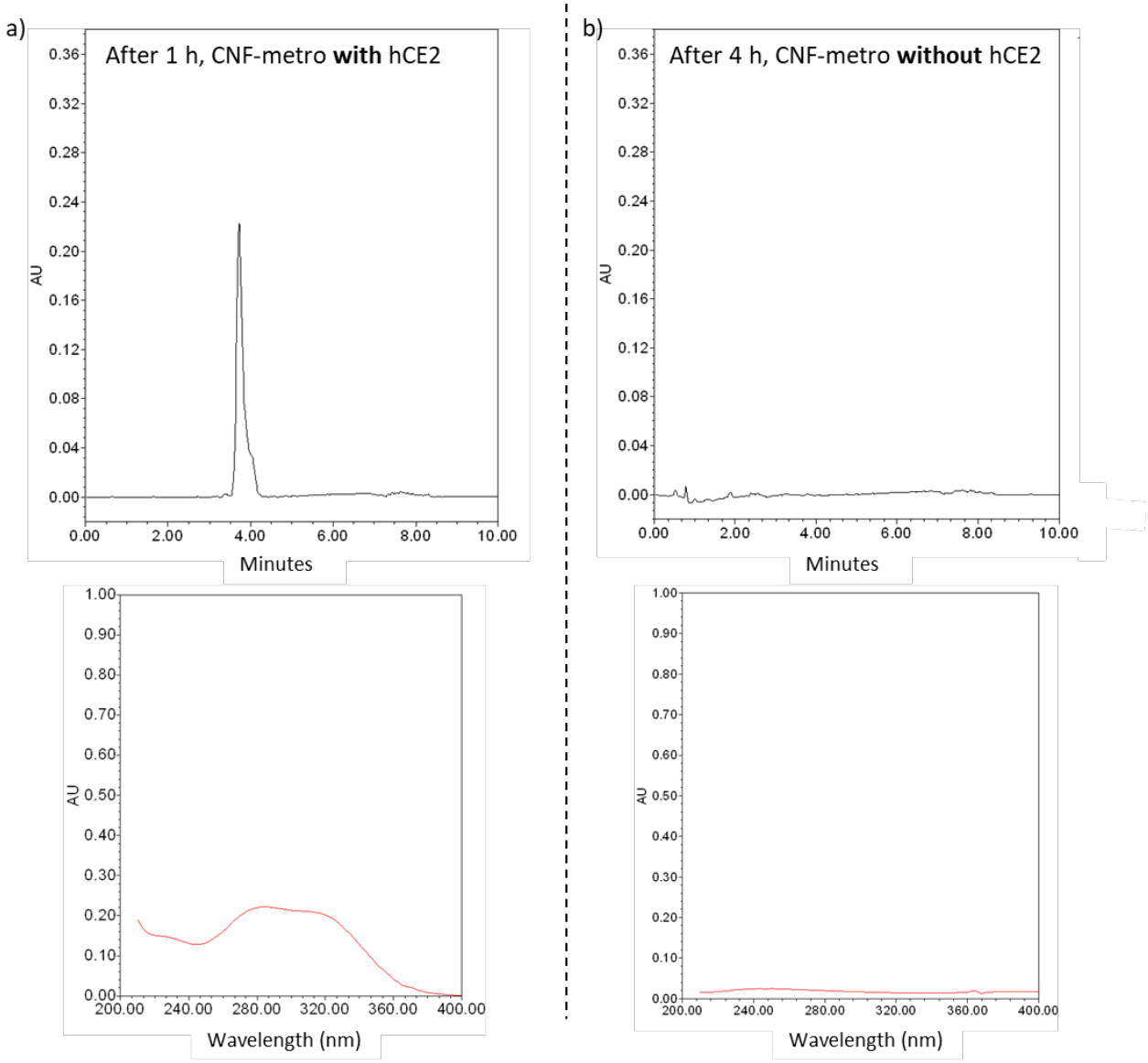

Figure 9: HPLC chromatograms (diode-array detector) (top) and associated UV spectra (bottom) of CNF-metro suspensions reacted a) with, and b) without the presence of carboxylesterase human 2 (hCE2)

This preliminary studies would deserve more investigation however the main outcome is that CNF-metro suspension, when exposed to hCE2 enzyme, is able to release metronidazole molecule in one hour. This result validates our starting hypothesis of controlled release of metronidazole from CNF under enzymatic activity.

Conclusion

In this work, a multistep immobilization procedure was proposed to graft thiol modified metronidazole prodrug onto TEMPO oxidized cellulose nanofibrils. The first step was an amidation reaction between carboxylic acid groups of CNF-t mainly confirmed by Raman spectroscopy, Solid state NMR and especially DNP enhanced NMR, with 2D analysis. Thus, an alkyne function was introduced at the surface of CNF. This key intermediate alkyne CNF opened the way to a range of chemical functionalization such as the thiol-yne reaction with thiol containing metronidazole prodrug described here, or a Michael-type addition of a suitably thiol- or amine-substituted prodrug. The presence of the prodrug was then confirmed by elemental analysis, conventional solid-state NMR and, more importantly DNP enhanced NMR that appeared as the ultimate tool to confirm the covalent nature of the grafting of the prodrug onto CNF substrates. These results further expand the strength of DNP enhanced NMR in the field of material characterization. Finally, the in situ drug release, arising from the presence of the cleavable ester function, was validated with the human carboxylesterase 2 medium, thus confirming that the presence of the CNF material did not prevent the enzyme activity. Following this work, the modified CNF system can be implemented in the design of innovative medical devices. Inspiring from commercial collagen-based implantable meshes, a composite of the prodrug modified CNF and collagen has been prepared to obtain an in situ triggered release of the drug (data not shown). The prototypes shows efficient preliminary antibacterial activity against anaerobic bacteria, confirming the particular potential of CNF-based medical devices in implantable applications.

Supporting information

The following data may be found in the Supporting Information file

- Conductometric titration of CNF-yne
- Detailed calculation for DO_{res}, $\%COOH_{conv.}$ and DS_{cond}
- Liquid ^{1}H and liquid ^{13}C NMR methods
- Prodrug characterization
- Solid state ^{13}C NMR on CNF-t, CNF-yne and CNF-metro
- 2D INADEQUATE for amidation confirmation

Acknowledgements

The authors thanks Univ. Grenoble Alpes, CNRS, Grenoble INP, LGP2, F-38000 Grenoble, France, and the French National Research Agency (ANR) (CELLICAL, ANR-15-CE08-0033, Arcane ANR-11-LABX-0003-01 and Glyco@Alps ANR-15-IDEX-02) for financial and technical supports.

We also thank A. Crisci from SIMAP, Grenoble who performed RAMAN spectroscopy measurements and ICR, Aix-Marseille University, UMR 7273, for the AMUPol biradical compound used in DNP-NMR

Fot the DNP-ssNMR analysis, M. Bardet was supported by an Outgoing CEA fellowship from the CEA-Enhanced Eurotalents program, co-funded by FP7 Marie-Skłodowska-Curie COFUND program (Grant Agreement 600382) and financial support ERC Advanced Grant No. 320860

References

Agarwal, U. P. (2017). Raman Spectroscopy of CNC-and CNF-Based Nanocomposites. *Handbook of Nanocellulose and Cellulose Nanocomposites*, 609–625.

Aulin, C., Gällstedt, M., & Lindström, T. (2010). Oxygen and oil barrier properties of microfibrillated cellulose films and coatings. *Cellulose*, *17*(3), 559–574. https://doi.org/10.1007/s10570-009-9393-y

Bardet, R., & Bras, J. (2014). Cellulose Nanofibers and Their Use in Paper Industry. In K. Oksman, A. P. Mathew, A. Bismarck, O. Rojas, & M. Sain, *Materials and Energy* (Vol. 5, pp. 207–232). WORLD SCIENTIFIC. https://doi.org/10.1142/9789814566469_0013

Bliman, D., Demeunynck, M., Leblond, P., Meignan, S., Baussane, I., & Fort, S. (2018). Enzymatically Activated Glyco-Prodrugs of Doxorubicin Synthesized by a Catalysis-Free Diels–Alder Reaction. *Bioconjugate Chemistry*, *29*(7), 2370–2381. https://doi.org/10.1021/acs.bioconjchem.8b00314

Boufi, S., González, I., Delgado-Aguilar, M., Tarrès, Q., Pèlach, M. À., & Mutjé, P. (2016). Nanofibrillated cellulose as an additive in papermaking process: A review. *Carbohydrate Polymers*, *154*, 151–166. https://doi.org/10.1016/j.carbpol.2016.07.117

Cadars, S., Sein, J., Duma, L., Lesage, A., Pham, T. N., Baltisberger, J. H., Brown, S. P., & Emsley, L. (2007). The refocused INADEQUATE MAS NMR experiment in multiple spin-systems: Interpreting observed correlation peaks and optimising lineshapes. *Journal of Magnetic Resonance (San Diego, Calif.: 1997)*, *188*(1), 24–34. https://doi.org/10.1016/j.jmr.2007.05.016

595 Campos-Aldrete, M. E., & Villafuerte-Robles, L. (1997). Influence of the viscosity grade and the particle
596 size of HPMC on metronidazole release from matrix tablets. *European Journal of*
597 *Pharmaceutics and Biopharmaceutics*, *43*(2), 173–178. https://doi.org/10.1016/S0939-
598 6411(96)00004-5
599 Celebi, D., Guy, R. H., Edler, K. J., & Scott, J. L. (2016). Ibuprofen delivery into and through the skin from
600 novel oxidized cellulose-based gels and conventional topical formulations. *Int. J. Pharm.*,
601 *514*(1), 238–243. https://doi.org/10.1016/j.ijpharm.2016.09.028
602 da Silva Perez, D., Montanari, S., & Vignon, M. R. (2003). TEMPO-Mediated Oxidation of Cellulose III.
603 *Biomacromolecules*, *4*(5), 1417–1425. https://doi.org/10.1021/bm034144s
604 Du, H., Liu, W., Zhang, M., Si, C., Zhang, X., & Li, B. (2019). Cellulose nanocrystals and cellulose
605 nanofibrils based hydrogels for biomedical applications. *Carbohydrate Polymers*, *209*, 130–
606 144. https://doi.org/10.1016/j.carbpol.2019.01.020
607 Dufresne, A., Thomas, S., & Pothan, L. A. (2013). *Biopolymer Nanocomposites: Processing, Properties,*
608 *and Applications*. John Wiley & Sons.
609 Fujisawa, S., Okita, Y., Saito, T., Togawa, E., & Isogai, A. (2011). Formation of N-acylureas on the surface
610 of TEMPO-oxidized cellulose nanofibril with carbodiimide in DMF. *Cellulose*, *18*(5), 1191.
611 https://doi.org/10.1007/s10570-011-9578-z
612 Fung, B. M., Khitrin, A. K., & Ermolaev, K. (2000). An Improved Broadband Decoupling Sequence for
613 Liquid Crystals and Solids. *Journal of Magnetic Resonance*, *142*(1), 97–101.
614 https://doi.org/10.1006/jmre.1999.1896
615 Gates, K. A., Grad, H., Birek, P., & Lee, P. I. (1994). A New Bioerodible Polymer Insert for the Controlled
616 Release of Metronidazole. *Pharmaceutical Research*, *11*(11), 1605–1609.
617 https://doi.org/10.1023/A:1018913921956
618 Guo, J., Filpponen, I., Johansson, L.-S., Heiβler, S., Li, L., Levkin, P., & Rojas, O. J. (2018). Micro-patterns
619 on nanocellulose films and paper by photo-induced thiol–yne click coupling: A facile method

toward wetting with spatial resolution. *Cellulose*, *25*(1), 367–375. https://doi.org/10.1007/s10570-017-1593-2

Habibi, Y. (2014). Key advances in the chemical modification of nanocelluloses. *Chem. Soc. Rev.*, *43*(5), 1519–1542. https://doi.org/10.1039/C3CS60204D

Halib, N., Perrone, F., Cemazar, M., Dapas, B., Farra, R., Abrami, M., Chiarappa, G., Forte, G., Zanconati, F., Pozzato, G., Murena, L., Fiotti, N., Lapasin, R., Cansolino, L., Grassi, G., & Grassi, M. (2017). Potential Applications of Nanocellulose-Containing Materials in the Biomedical Field. *Materials*, *10*(8), 977. https://doi.org/10.3390/ma10080977

Hoeng, F., Denneulin, A., & Bras, J. (2016). Use of nanocellulose in printed electronics: A review. *Nanoscale*, *8*(27), 13131–13154. https://doi.org/10.1039/C6NR03054H

Hoeng, F., Denneulin, A., Neuman, C., & Bras, J. (2015). Charge density modification of carboxylated cellulose nanocrystals for stable silver nanoparticles suspension preparation. *J. Nanoparticle Res.*, *17*(6). https://doi.org/10.1007/s11051-015-3044-z

Isogai, A., Saito, T., & Fukuzumi, H. (2011). TEMPO-oxidized cellulose nanofibers. *Nanoscale*, *3*(1), 71–85. https://doi.org/10.1039/C0NR00583E

Itiola, O. A., & Pilpel, N. (1986). Tableting characteristics of metronidazole formulations. *Int. J. Pharm.*, *31*(1), 99–105. https://doi.org/10.1016/0378-5173(86)90218-8

Johan Foster, E., J. Moon, R., P. Agarwal, U., J. Bortner, M., Bras, J., Camarero-Espinosa, S., J. Chan, K., D. Clift, M. J., D. Cranston, E., J. Eichhorn, S., M. Fox, D., Y. Hamad, W., Heux, L., Jean, B., Korey, M., Nieh, W., J. Ong, K., S. Reid, M., Renneckar, S., … Youngblood, J. (2018). Current characterization methods for cellulose nanomaterials. *Chem. Soc. Rev.*, *47*(8), 2609–2679. https://doi.org/10.1039/C6CS00895J

Jorfi, M., & Foster, E. J. (2015). Recent advances in nanocellulose for biomedical applications. *Journal of Applied Polymer Science*, *132*(14), n/a-n/a. https://doi.org/10.1002/app.41719

Kargarzadeh, H., Mariano, M., Gopakumar, D., Ahmad, I., Thomas, S., Dufresne, A., Huang, J., & Lin, N. (2018). Advances in cellulose nanomaterials. *Cellulose*, *25*(4), 2151–2189. https://doi.org/10.1007/s10570-018-1723-5

Kolb, H. C., Finn, M. G., & Sharpless, K. B. (2001). Click Chemistry: Diverse Chemical Function from a Few Good Reactions. *Angewandte Chemie International Edition*, *40*(11), 2004–2021. https://doi.org/10.1002/1521-3773(20010601)40:11<2004::AID-ANIE2004>3.0.CO;2-5

Kumar, A., Durand, H., Zeno, E., Balsollier, C., Watbled, B., Sillard, C., Fort, S., Baussanne, I., Belgacem, N., Lee, D., Hediger, S., Demeunynck, M., Bras, J., & De Paëpe, G. (2020). The surface chemistry of a nanocellulose drug carrier unravelled by MAS-DNP. *Chemical Science*, *11*(15), 3868–3877. https://doi.org/10.1039/C9SC06312A

Laurén, P. (2018). *Biomedical applications of nanofibrillar cellulose (Ph.D. thesis)*. https://www.google.com/url?sa=t&rct=j&q=&esrc=s&source=web&cd=1&ved=2ahUKEwjOtPzOjsPfAhWuTxUIHbgSAZAQFjAAegQIBhAC&url=https%3A%2F%2Fhelda.helsinki.fi%2Fbitstream%2Fhandle%2F10138%2F235619%2FBiomedic.pdf%3Fsequence%3D1%26isAllowed%3Dy&usg=AOvVaw3GZ5igbi7YuuPcEB1TFcgA

Lavoine, N., Bras, J., Saito, T., & Isogai, A. (2017). Optimization of preparation of thermally stable cellulose nanofibrils via heat-induced conversion of ionic bonds to amide bonds. *Journal of Polymer Science Part A: Polymer Chemistry*, *55*(10), 1750–1756. https://doi.org/10.1002/pola.28541

Lavoine, N., Desloges, I., Manship, B., & Bras, J. (2015). Antibacterial paperboard packaging using microfibrillated cellulose. *J. Food Sci. Technol.*, *52*(9), 5590–5600.

Lesage, A., Bardet, M., & Emsley, L. (1999). Through-Bond Carbon−Carbon Connectivities in Disordered Solids by NMR. *Journal of the American Chemical Society*, *121*(47), 10987–10993. https://doi.org/10.1021/ja992272b

Lin, N., & Dufresne, A. (2014). Nanocellulose in biomedicine: Current status and future prospect. *European Polymer Journal*, *59*, 302–325. https://doi.org/10.1016/j.eurpolymj.2014.07.025

Mangiante, G., Alcouffe, P., Burdin, B., Gaborieau, M., Zeno, E., Petit-Conil, M., Bernard, J., Charlot, A., & Fleury, E. (2013). Green Nondegrading Approach to Alkyne-Functionalized Cellulose Fibers and Biohybrids Thereof: Synthesis and Mapping of the Derivatization. *Biomacromolecules*, *14*(1), 254–263. https://doi.org/10.1021/bm3016829

Metronidazole: MedlinePlus Drug Information. (n.d.). Retrieved August 30, 2018, from https://medlineplus.gov/druginfo/meds/a689011.html

Missoum, K., Belgacem, M. N., & Bras, J. (2013). Nanofibrillated Cellulose Surface Modification: A Review. *Materials*, *6*(5), 1745–1766. https://doi.org/10.3390/ma6051745

Montanari, S., Roumani, M., Heux, L., & Vignon, M. R. (2005). Topochemistry of Carboxylated Cellulose Nanocrystals Resulting from TEMPO-Mediated Oxidation. *Macromolecules*, *38*(5), 1665–1671. https://doi.org/10.1021/ma048396c

Navarro, J. R. G., Conzatti, G., Yu, Y., Fall, A. B., Mathew, R., Edén, M., & Bergström, L. (2015). Multicolor Fluorescent Labeling of Cellulose Nanofibrils by Click Chemistry. *Biomacromolecules*, *16*(4), 1293–1300. https://doi.org/10.1021/acs.biomac.5b00083

Nordli, H. R., Chinga-Carrasco, G., Rokstad, A. M., & Pukstad, B. (2016). Producing ultrapure wood cellulose nanofibrils and evaluating the cytotoxicity using human skin cells. *Carbohydrate Polymers*, *150*, 65–73. https://doi.org/10.1016/j.carbpol.2016.04.094

Pahimanolis, N., Hippi, U., Johansson, L.-S., Saarinen, T., Houbenov, N., Ruokolainen, J., & Seppälä, J. (2011). Surface functionalization of nanofibrillated cellulose using click-chemistry approach in aqueous media. *Cellulose*, *18*(5), 1201–1212. https://doi.org/10.1007/s10570-011-9573-4

Paukkonen, H., Kunnari, M., Laurén, P., Hakkarainen, T., Auvinen, V.-V., Oksanen, T., Koivuniemi, R., Yliperttula, M., & Laaksonen, T. (2017). Nanofibrillar cellulose hydrogels and reconstructed hydrogels as matrices for controlled drug release. *International Journal of Pharmaceutics*, *532*(1), 269–280. https://doi.org/10.1016/j.ijpharm.2017.09.002

Pubchem. (n.d.). *Metronidazole*. Retrieved August 30, 2018, from https://pubchem.ncbi.nlm.nih.gov/compound/4173

Rol, F., Belgacem, M. N., Gandini, A., & Bras, J. (2018). Recent advances in surface-modified cellulose nanofibrils. *Progress in Polymer Science*. https://doi.org/10.1016/j.progpolymsci.2018.09.002

Rossini, A. J., Zagdoun, A., Lelli, M., Lesage, A., Copéret, C., & Emsley, L. (2013). Dynamic Nuclear Polarization Surface Enhanced NMR Spectroscopy. *Accounts of Chemical Research*, *46*(9), 1942–1951. https://doi.org/10.1021/ar300322x

Saito, T., Nishiyama, Y., Putaux, J.-L., Vignon, M., & Isogai, A. (2006). Homogeneous Suspensions of Individualized Microfibrils from TEMPO-Catalyzed Oxidation of Native Cellulose. *Biomacromolecules*, *7*(6), 1687–1691. https://doi.org/10.1021/bm060154s

Schakenraad, J. M., Hardonk, M. J., Feijen, J., Molenaar, I., & Nieuwenhuis, P. (1990). Enzymatic activity toward poly(L-lactic acid) implants. *Journal of Biomedical Materials Research*, *24*(5), 529–545. https://doi.org/10.1002/jbm.820240502

Sharma, K. S., Durand, G., Giusti, F., Olivier, B., Fabiano, A.-S., Bazzacco, P., Dahmane, T., Ebel, C., Popot, J.-L., & Pucci, B. (2008). Glucose-Based Amphiphilic Telomers Designed to Keep Membrane Proteins Soluble in Aqueous Solutions: Synthesis and Physicochemical Characterization. *Langmuir*, *24*(23), 13581–13590. https://doi.org/10.1021/la8023056

Solin, K., Orelma, H., Borghei, M., Vuoriluoto, M., Koivunen, R., & Rojas, O. J. (2019). Two-Dimensional Antifouling Fluidic Channels on Nanopapers for Biosensing. *Biomacromolecules*, *20*(2), 1036–1044. https://doi.org/10.1021/acs.biomac.8b01656

Syverud, K. (2016, spring). *SciFinder—Potential of cellulose nanofibrils in tissue engineering—ACS abstract*. https://scifinder-cas-org.gaelnomade.ujf-grenoble.fr/scifinder/view/scifinder/scifinderExplore.jsf

Valo, H., Arola, S., Laaksonen, P., Torkkeli, M., Peltonen, L., Linder, M. B., Serimaa, R., Kuga, S., Hirvonen, J., & Laaksonen, T. (2013). Drug release from nanoparticles embedded in four different nanofibrillar cellulose aerogels. *European Journal of Pharmaceutical Sciences*, *50*(1), 69–77. https://doi.org/10.1016/j.ejps.2013.02.023